# COMPUTATIONAL FLUID DYNAMICS SIMULATION OF LENGTH TO DIAMETER RATIO EFFECTS ON THE ENERGY SEPARATION IN A VORTEX TUBE

by

***Abdol Reza BRAMO*** [*] ***and Nader POURMAHMOUD***

Department of Mechanical Engineering, Urmia University, Urmia, Iran

Original scientific paper
UDC: 621.573:517.958
DOI: 10.2298/TSCI101004008B

*The objective of the present computational fluid dynamics analysis is an attempt to investigate the effect of length to diameter ratio on the fluid flow characteristics and energy separation phenomenon inside the Ranque-Hilsch vortex tube. In this numerical study, performance of Ranque-Hilsch vortex tubes, with length to diameter ratios of 8, 9.3, 10.5, 20.2, 30.7, and 35 with six straight nozzles was investigated. It includes generating better understanding of the effects of the stagnation point location on the performance of Ranque-Hilsch vortex tubes. It was found that the best performance was obtained when the ratio of vortex tube length to the diameter was 9.3 and also fort this case the stagnation point was found to be the farthest from the inlet. The results show that the closer distance to the hot end is produced the larger magnitude of the temperature difference. Computed results show good agreement with published experimental results.*

Key words: *Ranque-Hilsch vortex tube, computational fluid dynamics simulation, stagnation point, energy separation, thermal performance*

## Introduction

Ranque-Hilsch vortex tube is a simple device, which can produce temperature separation. When a vortex tube is supplied with compressed air through tangential nozzles in its vortex chamber, a strong rotational flow field is established. Due to wall friction, the velocity of gas near the tube wall is lower than the velocity at the tube center; as a result, gas in the center region transfers energy to the gas at the tube wall. After energy separation in the vortex tube, the inlet air stream gets separated in two streams: a hot air stream and a cold air stream; the hot air stream leaves the tube from one end and the cold air stream leaves from another end. Figure 1 shows a schematic diagram of a vortex tube and its flow patterns. Vortex tubes were discovered in 1932 by Ranque [1] and later Hilsch [2] performed the detailed examination of the so-called Ranque effect. Since then, the vortex tube has been a subject of much interest. Harnett *et al.* [3] invoked turbulence, Ahlborn *et al.* [4] described an embedded secondary circulation, and Stephan *et al.* [5] proposed the formation of Gortler vortices along the inside wall of the vortex tube. Kurosaka [6] reported the temperature separation to be a result of acoustic streaming effect. Aljuwayhel *et al.* [7] utilized a fluid

* Corresponding author; e-mail: rezabramo@yahoo.com

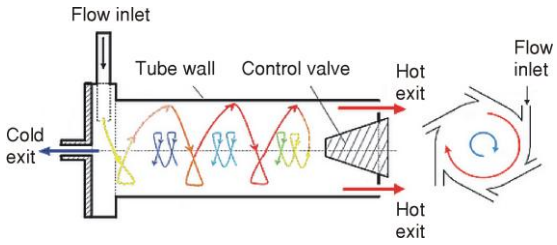


**Figure 1. Flow pattern and schematic diagram of vortex tube**

dynamics model of the vortex tube to study the flow behavior. Skye *et al.* [8] used a model similar to Aljuwayhel *et al.* [7]. Chang *et al.* [9] conducted an experiment using surface tracing method to investigation the flow field and to indicate the stagnation position in a vortex tube. Akhesmeh *et al.* [10] and Eisma *et al.* [11] performed a numerical simulation to study the flow field and temperature separation phenomenon. Kirmaci [12] employed a different method to optimize the nozzles number. Nezhad *et al.* [13] used a computational fluid dynamics (CFD) model to study the mechanism of flow and heat transfer in the vortex tube. Recently some studies have been done to use vortex tube as a refrigeration system instead of the conventional refrigeration systems [14, 15]. Vortex tubes generally are used as a cooling system for industrial purposes [16].

## Numerical modeling of vortex tube

The numerical simulation of the vortex tube has been created by using the FLUENT$^{TM}$ software package. The flow is assumed as 3-D, steady-state and employs the standard $k$-$\varepsilon$ turbulence model. The RNG $k$-$\varepsilon$ turbulence model and more advanced turbulence models such as the Reynolds stress equations were also investigated, but these models could not be made to converge for this simulation. Also, the $k$-$\omega$ and SST turbulence models were investigated, but results did not show the model accuracy relative to the experimental data; the analysis results are put in figs. 2 and 3. As seen in fig. 3, the obtained results for hot gas temperature $T_h$, are in good agreement with the experimental data in all studied models. As represented in fig. 2, for the obtained results at cold gas temperature $T_c$, the $k$-$\varepsilon$ model shows better agreement with experimental data in comparison with the other studied models. Due to the good agreement with the experimental data the $k$-$\varepsilon$ model was selected to simulate the effect of turbulence inside of vortex tube system. The compressible turbulent flows in this machine are governed by the conservation of mass, momentum, and energy equations, which are given by:

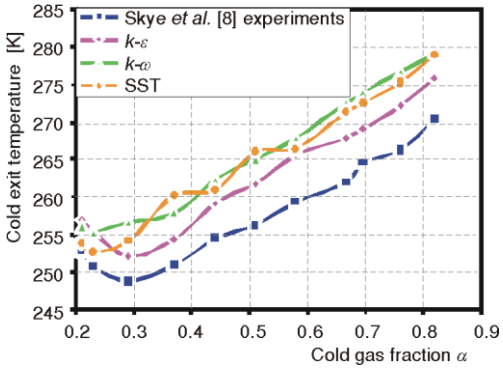


**Figure 2. The outlet cold gas temperature obtained at different turbulence models**

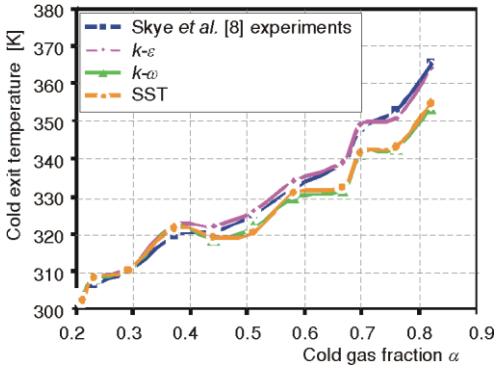


**Figure 3. The outlet hot gas temperature obtained at different turbulence models**

$$\frac{\partial}{\partial x_j}(\rho u_j) = 0 \tag{1}$$

$$\frac{\partial}{\partial x_j}(\rho u_i u_j) = -\frac{\partial p}{\partial x_i} + \frac{\partial}{\partial x_j}\left[\mu\left(\frac{\partial u_i}{\partial x_j} + \frac{\partial u_j}{\partial x_i} - \frac{2}{3}\delta_{ij}\frac{\partial u_k}{\partial x_k}\right)\right] + \frac{\partial}{\partial x_j}(-\overline{\rho' u_i' u_j'}) \tag{2}$$

$$\frac{\partial}{\partial x_i}\left[u_i\rho\left(h + \frac{1}{2}u_j u_j\right)\right] = \frac{\partial}{\partial x_j}\left[k_{\text{eff}}\frac{\partial T}{\partial x_j} + u_i(\tau_{ij})_{\text{eff}}\right] \qquad k_{\text{eff}} = K + \frac{c_p\mu_t}{\text{Pr}_t} \tag{3}$$

Because of the compressibility effect, the state equation for an ideal gas is necessary and given as:

$$p = \rho RT \tag{4}$$

The flow field throughout the vortex tube is fully turbulent. Thus, the turbulence kinetic energy, $k$, and its rate of dissipation, $\varepsilon$, are obtained from the following transport equations:

$$\frac{\partial}{\partial t}(\rho k) + \frac{\partial}{\partial x_i}(\rho k u_i) = \frac{\partial}{\partial x_j}\left[\left(\mu + \frac{\mu_t}{\sigma_k}\right)\frac{\partial k}{\partial x_j}\right] + G_k + G_b - \rho\varepsilon - Y_M \tag{5}$$

$$\frac{\partial}{\partial t}(\rho k) + \frac{\partial}{\partial x_i}(\rho k u_i) = \frac{\partial}{\partial x_j}\left[\left(\mu + \frac{\mu_t}{\sigma_\varepsilon}\right)\frac{\partial \varepsilon}{\partial x_j}\right] + C_{1\varepsilon}\frac{\varepsilon}{k}(G_k + C_{3\varepsilon}G_b) - C_{2\varepsilon}\rho\frac{\varepsilon^2}{k} \tag{6}$$

where $G_k$ represents the generation of turbulence kinetic energy due to the mean velocity gradients and $G_b$ is the generation of turbulence kinetic energy due to buoyancy which is neglected in this case. $Y_M$ represents the contribution of the fluctuating in compressible turbulence to the overall dissipation rate and $C_{1\varepsilon}$, $C_{2\varepsilon}$, and $C_{3\varepsilon}$ are coefficients. $\sigma_k$ and $\sigma_\varepsilon$ are the turbulent Prandtl numbers for $k$ and $\varepsilon$, respectively. The turbulent viscosity, $\mu_t$, is computed by combining $k$ and $\varepsilon$ as:

$$\mu_t = \rho C_\mu \frac{k^2}{\varepsilon} \tag{7}$$

where $C_\mu$ is a constant. The model constants $C_{1\varepsilon}$, $C_{2\varepsilon}$, $C_\mu$, $\sigma_k$, and $\sigma_\varepsilon$ have the following default values: $C_{1\varepsilon} = 1.44$, $C_{2\varepsilon} = 1.92$, $C_\mu = 0.09$, $\sigma_k = 1.0$, and $\sigma_\varepsilon = 1.3$.

## Physical modeling

The present created CFD model is based on that was used by Skye *et al* [8]. It is noteworthy that, an Exair™ 708 slpm vortex tube (the geometry summary is given in tab. 1) was used by Skye to collect all of the experimental data and is shown in fig. 4. In addition to the model which was used by Skye, to study the effects of length on the performance of vortex tube, all geometrical properties of the Skye model are

**Table 1.Geometry summary of the vortex tube which was used in experiment**

| Measurement | Value |
|---|---|
| Working tube length | 106 mm |
| Nozzle height | 0.97 mm |
| Nozzle width | 1.41 mm |
| Nozzle total inlet area (An) | 8.2 mm$^2$ |
| Cold exit diameter | 6.2 mm |
| Cold exit area | 30.3 mm$^2$ |
| Hot exit diameter | 11 mm |
| Hot exit area | 95 mm$^2$ |

kept constant. By varying the length of the model, five other models with different lengths and six numbers of straight nozzles were created. The radius of the vortex tubes fixed at 5.7 m

m, and the length are set to 92, 106, 120, 230, 350, and 400 mm, respectively. Since the nozzle consists of 6 straight slots, the CFD model has been assumed to be a rotational periodic flow and only a sector of the flow domain with angle of 60°. The 3-D CFD model with refinement in mesh along with boundary regions is shown in fig. 5.

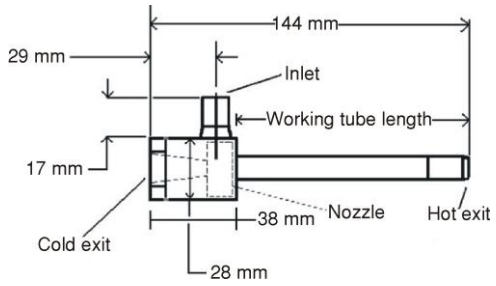


**Figure 4. Schematic drawing of simulated an Exair™ 708 slpm model vortex tube**

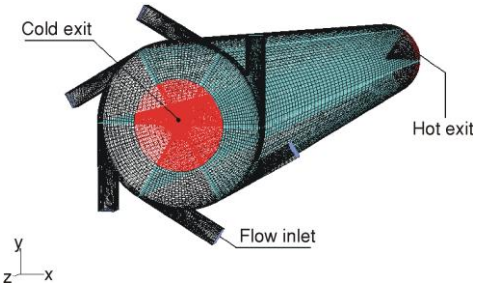


**Figure 5. Three-dimensional CFD model of vortex tube with six straight nozzles (color image see on our web site)**

*Grid dependence study*

To remove the errors due to coarseness of grids, analysis has been carried out for different average unit cell volumes in a vortex tube of length to diameter (*L/D)* ratio of 9.3. The variation of total temperature difference and maximum swirl velocity as key parameters are shown in fig. 6 and 7 for different unit cell volumes. It can be seen that not much advantage in reducing the unit cell volume size below 0.0257 mm$^3$ which corresponds to 0.287 million cells for the configuration studied.

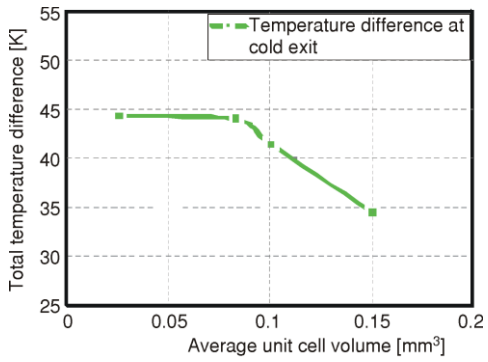


**Figure 6. Grid size dependence study on total temperature difference at different average unit cell volume**

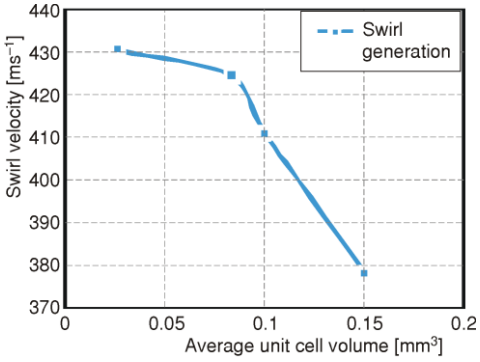


**Figure 7. Grid size dependence study on maximum swirl velocity at different average unit cell volume**

*Boundary conditions for analysis*

For all cases in this analysis, the simulation boundary conditions for the model were identified based on the experimental measurements by Skye. The inlet is modeled as a mass flow inlet. The specified total mass flow rate and stagnation temperature were fixed to 8.35 g/s and 294.2 K, respectively The static pressure at the cold exit boundary was fixed at experimental measurements pressure. The static pressure at the hot exit boundary is adjusted in the way to vary the cold mass fraction.

## Results and discussion

CFD analyses were carried out for a 11.4 mm diameter vortex tube with *L/D* of 8, 9.3, 10.5, 20.2, 30.7, and 35 to attain the optimum *L/D* ratio. The results shown that, the best performance is obtained when the length to diameter ratio is 9.3 ($L$ = 106 mm). Notice that this is the same model that was used by Skye. The obtained results for optimum case (106 mm) were compared and validated with experimental and numerical results (figs. 8 and 9).

*Effect of length to diameter ratio*

As illustrated in figs. 8 and 9, the obtained temperature difference at present analysis for the optimum vortex tube ($L$ = 106 mm), were compared with the experimental and computational results of [ ], that both models have similar geometry and boundary conditions. The Skye CFD model was developed in a 2-D form but the present CFD models are 3-D. In fig. 9 the $\Delta T_{h,i}$, is predicted by the model and is in good agreement with the experimental values. Prediction of the $\Delta T_{i,c}$ is found to be lie between the experimental and computational results of [8], which is shown in fig. 8. The simulated $\Delta T_{h,i}$ at both models were close to the experimental results. Though, both models get values lower than the experimental results of $\Delta T_{i,c}$, but the predictions from the present model was found closer to mentioned experiment. In fig. 8 the maximum $\Delta T_{i,c}$ is obtained at cold mass fraction of about 0.3 through the experiment and CFD simulation. The optimum vortex tube length ($L$ = 106 mm) can produce hot gas temperature of 363.2 K at 0.8 of cold mass fraction and a minimum cold gas temperature of 250.24 K at about 0.3 cold mass fraction.

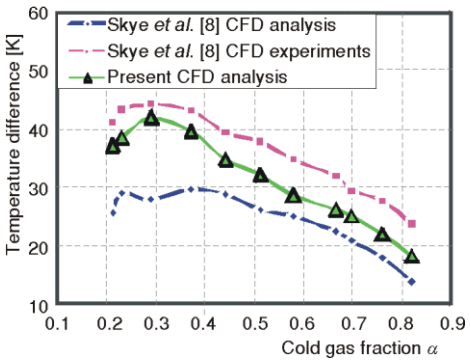


**Figure 8. Comparison of cold temperature differences obtained at present CFD simulation with experiments**

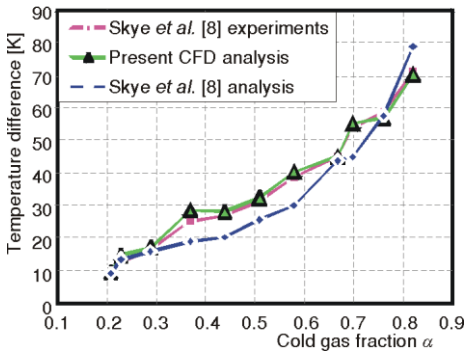


**Figure 9. Comparison of hot temperature differences obtained at present CFD simulation with experiments**

The analysis results for all vortex tube lengths that were investigated are given in tab. 2.

**Table 2.The results of CFD analysis for all vortex tubes lengths that were investigated at $\alpha = 0.3$ (maximum cooling effect)**

| $L/D$ | $L$ [mm] | $V_{sm}$ [ms$^{-1}$] | $T_{cm}$ [K] | $T_{hm}$ [K] | $\Delta T_{i,c}$ [K] | $\Delta T_{h,i}$ [K] | $\Delta T_{ch}$ [K] |
|---|---|---|---|---|---|---|---|
| 8 | 92 | 390 | 254.77 | 310.56 | 39.48 | 16.36 | 55.84 |
| 9.3 | 106 | 428 | 250.24 | 311.5 | 43.96 | 17.3 | 61.26 |
| 10.5 | 120 | 390 | 254.72 | 309.45 | 39.48 | 15.25 | 54.73 |
| 20.2 | 230 | 387 | 254.9 | 310.7 | 39.3 | 16.5 | 55.8 |
| 30.7 | 350 | 388 | 255.05 | 310.33 | 39.15 | 16.13 | 55.28 |
| 35 | 400 | 388 | 254.94 | 310.68 | 39.26 | 16.48 | 55.74 |

$V_{sm}$ – Maximum swirl velocity, $T_{cm}$ – Minimum temperature at cold end, $T_{hm}$ – Maximum temperature at hot end

In respect of varying tube length, radial profiles of axial velocity at different axial locations ($z/L$ = 0.1, 0.4, and 0.7) at specified cold mass fraction of 0.3 are displayed in fig. 10. For the optimum case at axial locations of $z/L$ = 0.1, 0.4, and 0.7 the maximum axial velocity was found 83, 63, and 57 m/s, respectively. Therefore, a maximum value of 83 m/s is seen at the tube axis near the inlet zone ($z/L$ = 0.1). The radial profiles for the swirl velocity

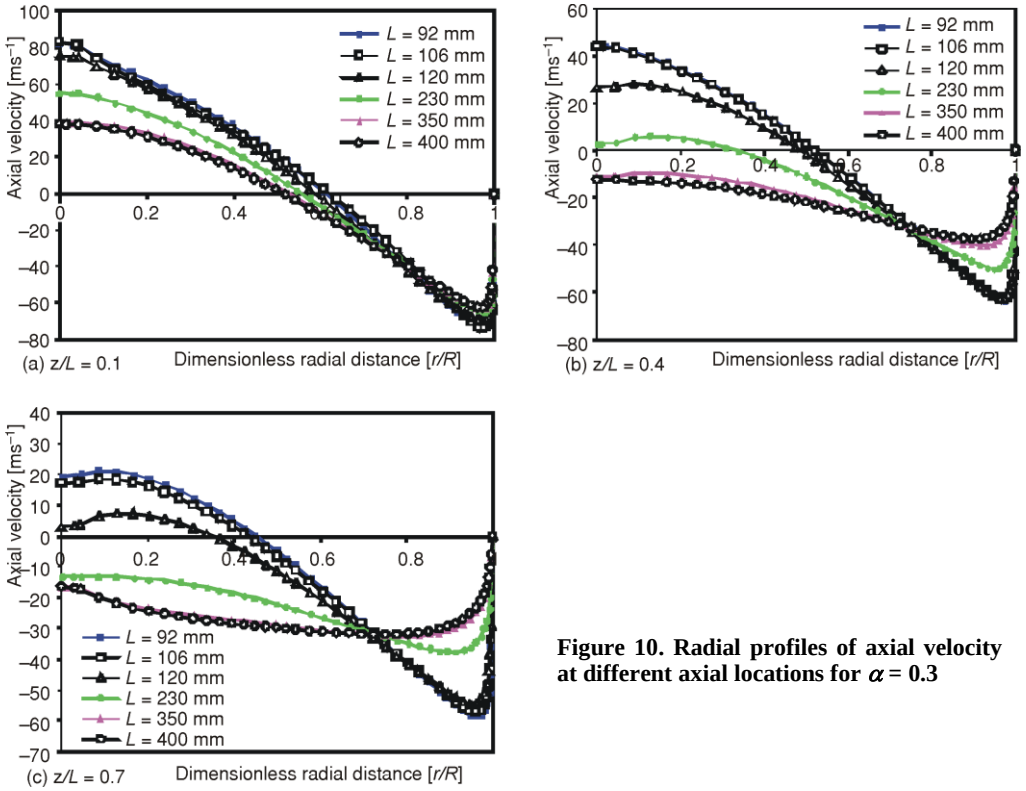


**Figure 10. Radial profiles of axial velocity at different axial locations for $\alpha = 0.3$**

at $z/L$ = 0.1, 0.4, and 0.7 is revealed in fig. 11. Comparing the velocity components, thus, it is cleared that swirl velocity has the highest value. The radial profile of the swirl velocity indicates a free vortex near the wall and the values become negligibly small at the core, which is in conformity with the observations of Kurosaka [6] and Gutsol [17]. Also, the obtained axial and swirl velocity profiles at different $z/L$ are in good conformity with observations of Gutsol [17] and Behera [18] in all models. Figure 11 shows in near of the inlet zone ($z/L$ = 0.1), and in comparing with other models the highest swirl velocity belongs to model with $L$ = 106 mm. Increasing the distance from inlet zone towards the hot end the swirl velocity magnitude decreases in all models**.**

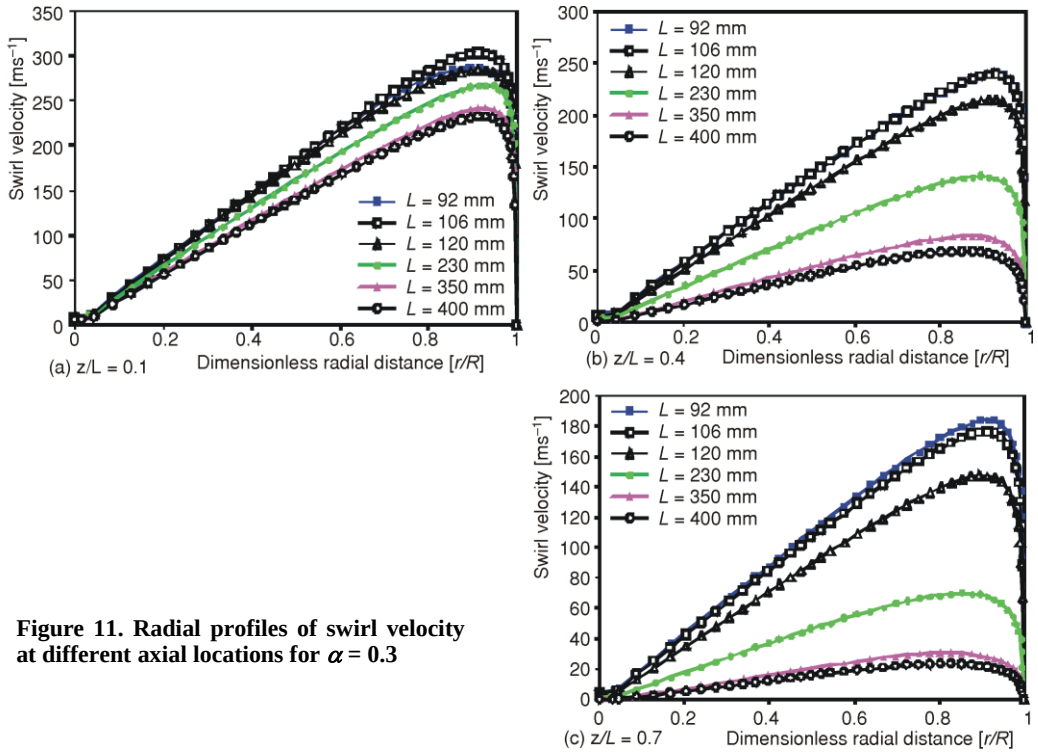


**Figure 11. Radial profiles of swirl velocity at different axial locations for $\alpha$ = 0.3**

The total temperature variations for different length of vortex tube are presented in fig. 12. The maximum total temperature was occurred near to the periphery of the tube wall in all vortex tubes. Comparing the total temperature and the swirl velocity profiles (figs. 11 and 12) show that the low temperature zone in the core coincides with the negligible swirl velocity zone. The total temperature profiles, fig. 12, show an increase of the temperature values towards the periphery. As seen in figs. 12(a) and (c), the model with $L$ = 106 mm shows minimum cold gas temperature at cold exit and maximum hot gas temperature at hot exit. The Radial variations of the total pressure for different lengths of vortex tube are seen in fig. 13. The most expansion occurs at the nozzle exit, which causes increase in velocity. After the working fluid entering the tube through the nozzles, the fluid expands up to stagnation point. Then, the gas expands again, up to cold outlet, where it drops to atmospheric pressure which causes increased velocity in this zone. The maximum total pressure is

appeared near the periphery of tube wall in all of the vortex tubes. Comparing the total temperature and the total pressure profiles (figs. 12 and 13) shows the low temperature zone in the core coincides with the low total pressure zone. The total pressure profiles (fig. 13) show an increase of the pressure values towards the periphery. Also, pressure drop increases with increasing of tube length especially at longer models.

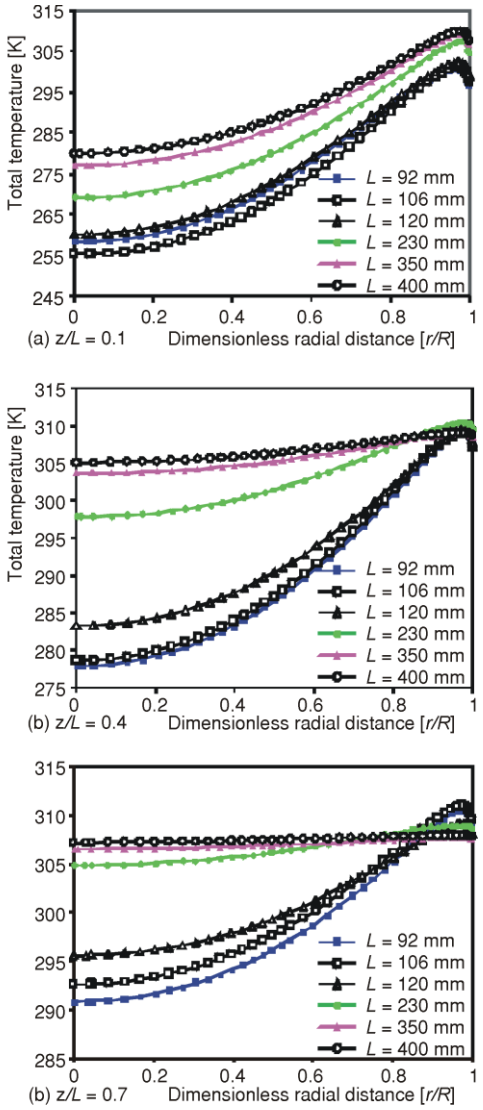


**Figure 12. Radial profiles of total temperature at different axial locations for $\alpha = 0.3$**

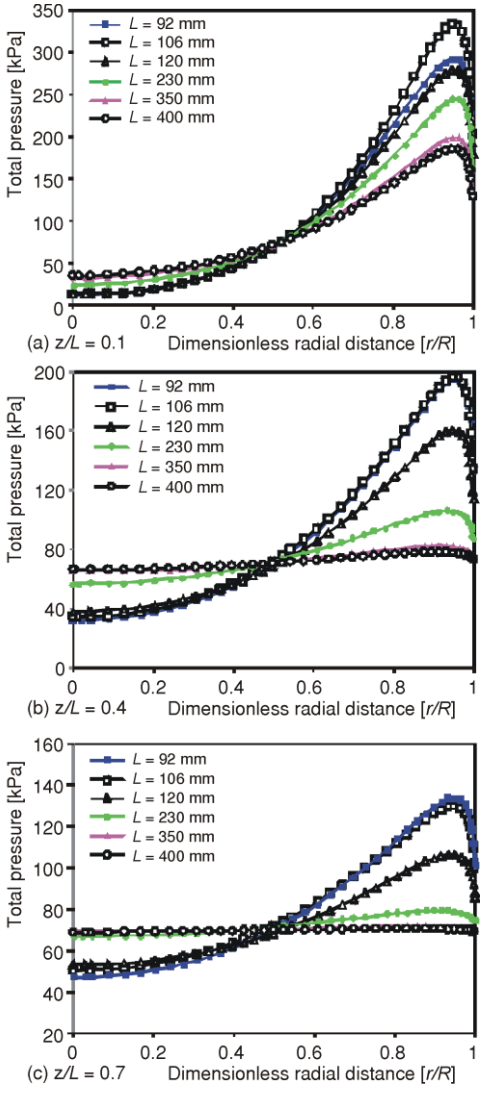


**Figure 13. Radial profiles of total pressure at different axial locations for $\alpha = 0.3$**

The total temperature distribution for optimized length ($L$ = 106 mm) is displayed in fig. 14. Clearly can be seen that peripheral flow is warm and core flow is cold. Furthermore,

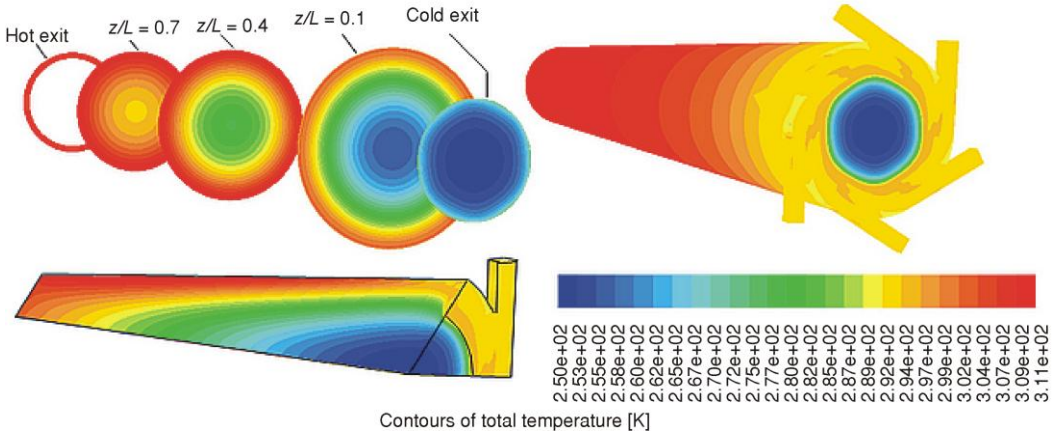


**Figure 14. Contours of total temperature at z/L = 0.1, z/L = 0.4, z/L = 0.7. (color image see on our web site)**

increasing of temperature is observed in radial direction. The optimum length of this study, for a cold mass fraction of about 0.3, gives the maximum hot gas temperature of 311.5 K and minimum cold gas temperature of 250.24 K. Figure 15 shows the CFD analysis data on temperature difference between hot and cold end ($\Delta T_{ch}$) for various *L/D* ratios. The peak value in $\Delta T_{ch}$, is obtained for *L/D* ratio of 9.3 (*L* = 106 mm) that was investigated experimentally by Skye. Figure 16 shows the temperature difference at cold exit end, $\Delta T_{i,c}$, for various lengths of vortex tube, which were investigated. Investigation of vortex tube length effect is indicated the model with length of 106 mm has the maximum temperature separation about 43.96 K at cold exit.

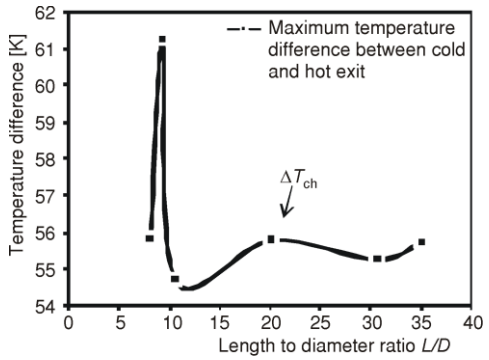


**Figure 15. Temperature difference between hot and cold gas for different *L/D* ratios**

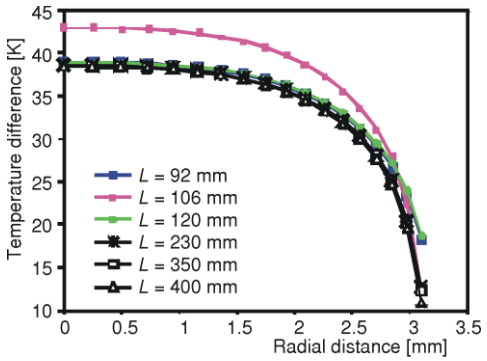


**Figure 16. Temperature difference at cold exit for different lengths of vortex tube**

As we know, vortex tube can be operated in such a way to produce maximum hot gas temperature or minimum cold gas temperature. Figures 17 and 18 show the maximum hot gas temperatures and the minimum cold gas temperatures, respectively, which obtained at various *L/D* ratios and specified cold mass fraction of 0.3 (maximum cooling effect).

According to these figures for different *L/D* ratios the optimum value of *L/D* ratio is able to get a maximum hot gas temperature of 311.5 K and a minimum cold gas temperature of 250.24 K.

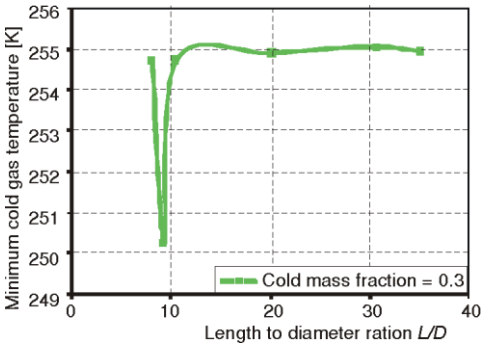


**Figure 17. Maximum hot gas temperature obtained at different *L/D* ratios**

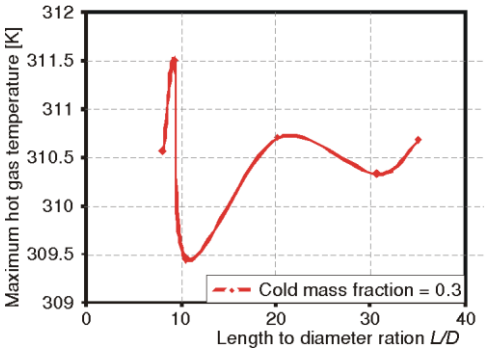


**Figure 18. Minimum cold gas temperature obtained at different *L/D* ratios**

*Effect of stagnation point*

The results of present study show that the performance of vortex tubes is related to stagnation point location and also, study on the length effect is required to explore of the stagnation point location along the tube to achieve the highest energy separation. Figure 19 shows the stagnation point and streamlines in the r–z plane associated with the flow inside the optimum vortex tube. As shown in fig. 20 the flow within the vortex tube has both of forced and free vortex flow regions up to stagnation point. The forced vortex is usually seen near the inlet region and the other one near to wall, which is in accordance with the observations of Kurosaka [6] and Gutsol [17]. As a result a free vortex is produced as the peripheral hot stream and a forced vortex as the inner cold stream.

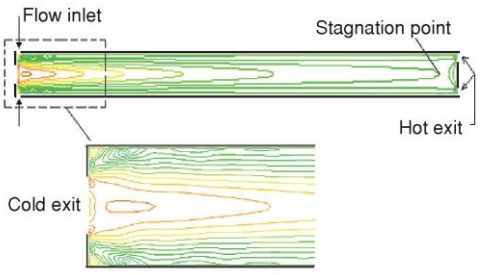


**Figure 19. Streamlines of optimum vortex tube in r–z plane**

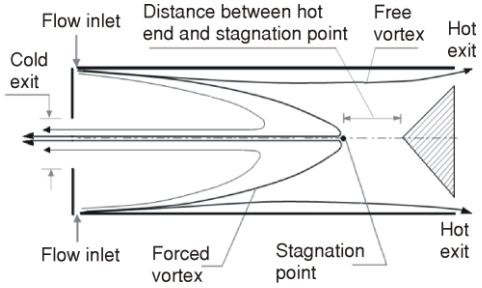


**Figure 20. Schematic flow pattern of Ranque-Hilsch vortex tube**

The stagnation point position within the vortex tube can be established from the velocity profile along the tube length at the point where axial velocity cease to have a negative value. Also, it can be established according to the maximum wall temperature, which this point represents the stagnation point described by Fulton [19]. It was assumed that the

wall temperature was representative of the gas temperature that reported by Frohlingsdorf [20].

The variations of axial velocity along the center line of the vortex tube are shown in fig. 21, where the *z/L* is represented as the dimensionless length of vortex tube. As indicated in this figure there is an axial distance between cold and hot ends that the velocity magnitude comes to zero. This point is specified as the stagnation point position.

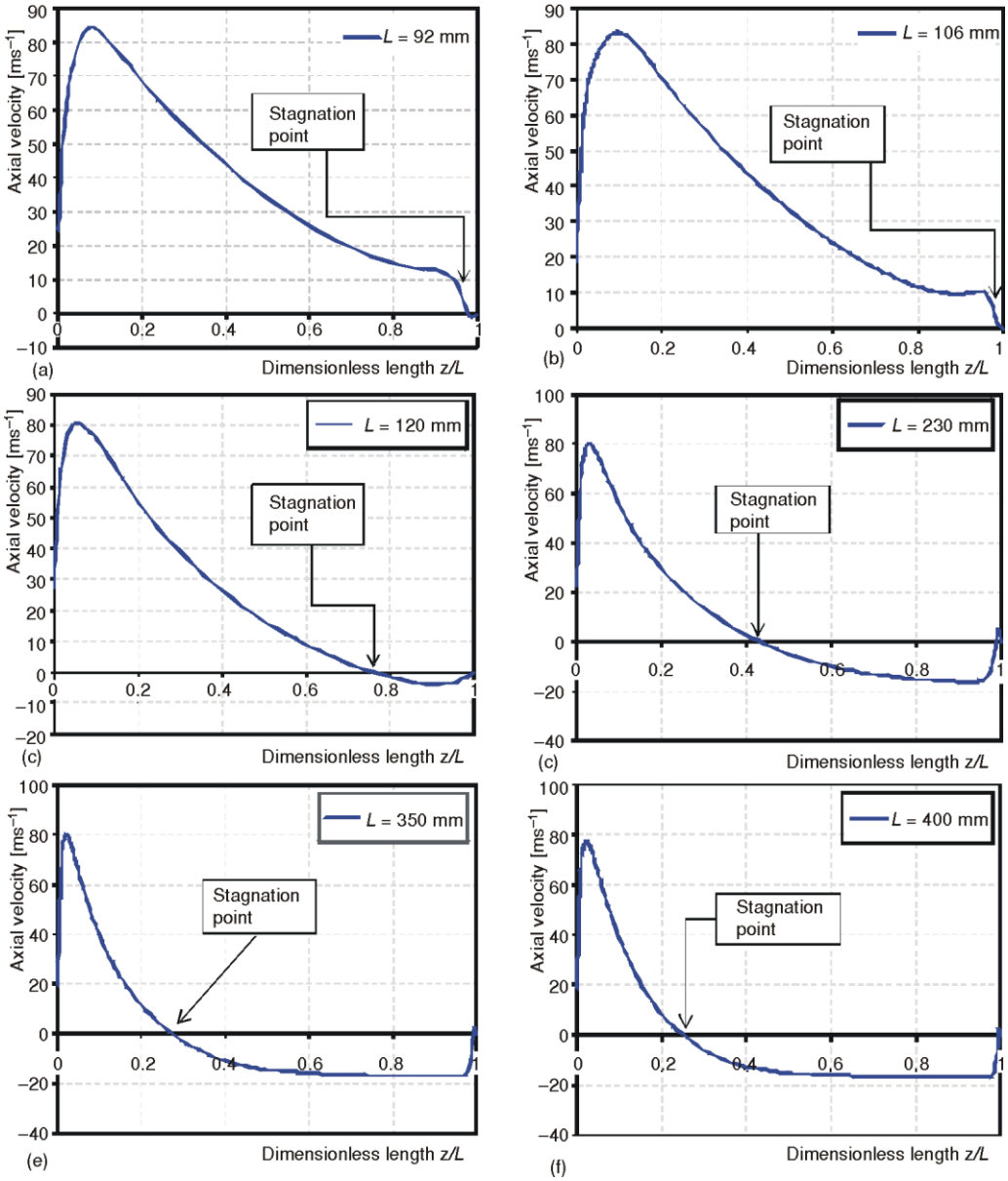


**Figure 21. Variation of axial velocity along the center line of the vortex tube**

From fig. 21, it can be seen that the stagnation point moves closer to the hot end as the length of tube increases. For the cases of $L \leq 120$ mm, the stagnation point takes place in the second half of the tube length, while for the values of $L \geq 270$ mm, the stagnation point rises in the first part of it. The exact predicted locations of the stagnation points are shown in tab. 3. In that figure the nearest stagnation point to the hot end belongs to vortex tube with $L$ = 106 mm (optimum case of present study). The results of analysis are represented the nearest stagnation point to the hot end gives the highest temperature difference which is an important point to get the best performance of vortex tubes. Also, it can be cited that with increasing the length of the vortex tube, stagnation point moves towards the cold exit end.

**Table 3. Stagnation point position along the vortex tube length for various length of tube**

| $L$ [mm] | $L/D$ | $L_{sc}$ [mm] | $D_{sh}$ [mm] | $z$/L | $\Delta T_{ch}$ [K] |
|---|---|---|---|---|---|
| 92 | 8 | 90.344 | 1.656 | 0.982 | 55.84 |
| 106 | 9.3 | 104.41 | 1.59 | 0.985 | 61.26 |
| 120 | 10.5 | 95.04 | 24.96 | 0.792 | 54.73 |
| 230 | 20.2 | 101.66 | 128.34 | 0.442 | 55.8 |
| 350 | 30.7 | 98.35 | 251.65 | 0.281 | 55.28 |
| 400 | 35 | 103.6 | 296.4 | 0.259 | 55.74 |

$L/D$ – Length to diameter ratio, $L_{sc}$ – Stagnation point location from cold end, $D_{sh}$ – Distance between hot end and stagnation point, ($z/L$) – Dimensionless tube length which is measured from the cold exit end

The variations of total temperature along the wall of the vortex tube at different lengths are given in fig. 22. In all cases in this figure the specified wall temperature can be interpreted as the stagnation point according to reports of Fulton *et al* [19]. Comparisons shown that the maximum wall temperature for vortex tube with lengths of 92, 106, and 120 mm is closer to the hot end. Also, notice that the obtained temperature differences in these models are greater than the other models. The results of present study about the position of stagnation point and its influence on the performance of vortex tube clearly confirms observation of Behera *et al.* [18].

In fig. 23 it has been endeavored to clear the reasons which make the maximum wall temperature as the stagnation point position. Physical mechanism of energy separation in vortex tube is related to exist of two counter flows in the tube.

Furthermore, due to friction effect the gas velocity in near tube wall is lower than the flow velocity at the tube center. Hence, after the energy separation the inlet gas is separated in two streams which are shown in fig. 23. One can conclude that as far as this point, the major value of energy transfer has occurred before stagnation point. This conclusion is coincide to reports of Aljuwayhel *et al.* [7]. They reported that there is a critical length for the vortex tube over which the majority of the energy transfers takes place under the conditions used in CFD models. The magnitude of the energy separation increases as the length of the vortex tube increases to a critical length. However, a further increase in the vortex tube length beyond the critical value will not improve the energy separation. In this study, CFD results have lead to determine of the length equal to 106 mm as critical length value.

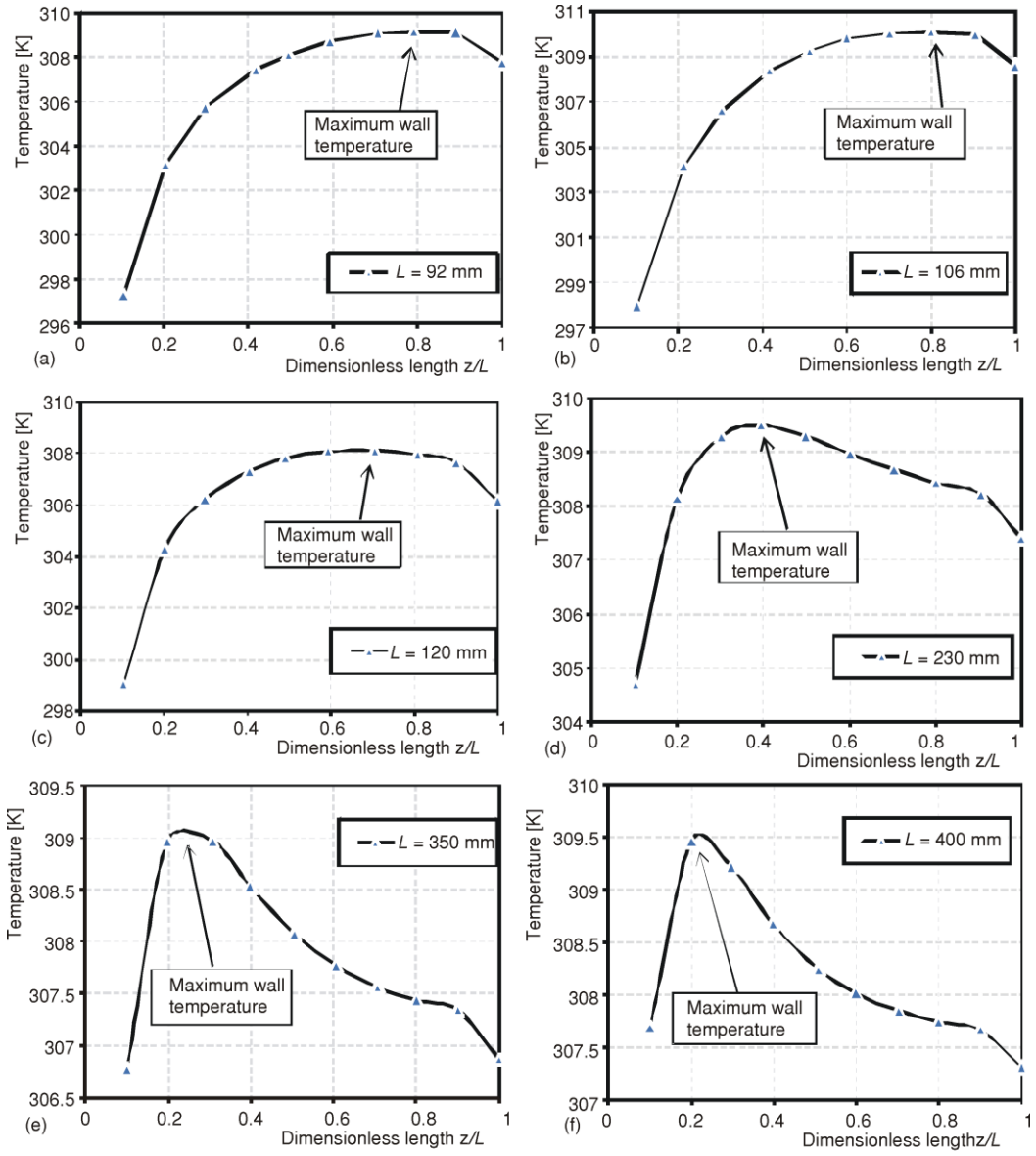


**Figure 22. The variations of wall temperature along the vortex tube length**

The obtained results of two methods to determine the position of the stagnation point are given and compared in tab. 4. By the numerical values of this table, the average difference between these two methods is about 14.8%. Comparison of two methods shows the obtained results by both methods present similar conclusion about the effects of stagnation point position on the energy separation within the vortex tube, so that in the both methods the farthest stagnation point from the inlet presents the highest temperature difference.

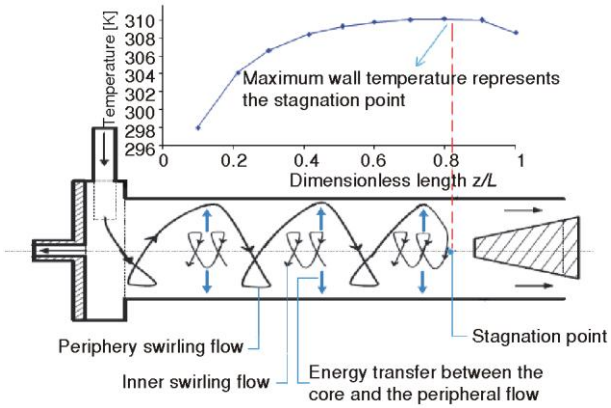


**Figure 23. Schematic description of energy transfer pattern in the vortex tube**

**Table 4. Comparison of the stagnation point location using two methods**

| $L$ [mm] | $L/D$ | $T_{wmax}$ | $(Z/L)_w$ | $(z/L)_v$ | Diff. [%] |
|---|---|---|---|---|---|
| 92 | 8 | 309.159 | 0.812286 | 0.982 | 17.2 |
| 106 | 9.3 | 310.119 | 0.834784 | 0.985 | 15.2 |
| 120 | 10.5 | 308.104 | 0.669506 | 0.792 | 15.5 |
| 230 | 20.2 | 309.517 | 0.38092 | 0.442 | 13.8 |
| 350 | 30.7 | 309.118 | 0.242601 | 0.281 | 13.6 |
| 400 | 35 | 309.485 | 0.223537 | 0.259 | 13.6 |

$T_{wmax.}$ – Maximum wall temperature, $(z/L)_w$ – Dimensionless distance of stagnation point based on measurement of wall temperature which is measured from the cold exit, $(z/L)_v$ – Dimensionless distance of stagnation point based on variation of axial velocity which is measured from the cold exit, Diff. – Difference between two measurement methods of stagnation point location

With respect of the obtained results by two methods, the optimum model of this study (vortex tube with $L$ = 106 mm) has the farthest stagnation point from the inlet at both methods.

## Conclusions

A numerical investigation is conducted to examine the performance of six vortex tubes which have an inner diameter of 11.4 mm and $L/D$ ratio of 8, 9.3, 10.5, 20.2, 30.7, and 35. The results shown that, the best performance is obtained when the length to diameter ratio is 9.3 ($L$ = 106 mm). Comparison of present numerical model and experimental data shows the hot and cold temperature difference in good agreement. Numerical results were closer to the experimental values compared to the Skye CFD model. The results show that increasing of the length to diameter ratio beyond 9.3 has no effect on the performance of vortex tube. For the optimum vortex tube length of this research it is possible to get a temperature difference between hot and cold streams as high as 61.26 K. The maximum cold temperature difference was obtained at 0.3 of cold mass fraction. It is concluded that to use vortex tube as a cooling system lower cold mass fraction is required.

The analysis show that the temperature difference between hot and cold gas flow can be improved by increasing the length of vortex tube such that stagnation point is farthest from the nozzle inlet and within the tube. In the optimum case of present study the stagnation point was found to be farthest from the inlet. It is observed that in the long length of vortex

tubes the stagnation point is far from the hot end and this affects the vortex tubes performance negatively.

Also both investigated methods to determine the stagnation point position, shown similar and reasonable results. So, to attain the large amounts of temperature separation in a vortex tube we recommended that the stagnation point must be in a minimum distance from the hot outlet.

## Nomenclature

$D$ – diameter of vortex tube, [m]
$K$ – conductivity coefficient, [$Wm^{-1}K^{-1}$]
$k$ – turbulence kinetic energy, [$m^2s^{-2}$]
$L$ – length of vortex tube, [m]
$\dot{M}$ – mass flow rate, [$gs^{-1}$]
$R$ – radial distance from axis, [m]
$T$ – temperature, [K]
$\Delta T_{ch}$ – temperature difference between cold and hot end, [K]
$\Delta T_{ic}$ – temperature difference between inlet and cold end, [K]
$\Delta T_{hi}$ – temperature difference between hot end and inlet, [K]
$u'$ – fluctuating component of velocity, [$ms^{-1}$]
$z$ – axial length from nozzle cross-section

*Greek symbols*

$\alpha$ – cold gas fraction
$\varepsilon$ – turbulence dissipation rate, [$m^2s^{-3}$]
$\delta_{ij}$ – Kronecker delta
$\rho$ – density, [$kgm^{-3}$]
$\sigma$ – stress, [$Nm^{-2}$]
$\mu$ – dynamic viscosity, [$kgm^{-1}s^{-1}$]
$\mu_t$ – turbulent viscosity, [$kgm^{-1}s^{-1}$]
$\tau$ – shear stress, [$Nm^{-2}$]
$\tau_{ij}$ – stress tensor components

## References

[1] Ranque, G. J., Experiments on Expansion in a Vortex with Simultaneous Exhaust of Hot Air and Cold Air (in French), *J. Phys.Radium*, *7* (1933), 4, pp. 112-114
[2] Hilsch, R., The Use of Expansion of Gases in Centrifugal Field as a Cooling Process (in German), *Rew Sci. Instrum*, *18* (1946), 2, pp. 208-214
[3] Hartnett, J., Eckert, E., Experimental Study of the Velocity and Temperature Distribution in a High- Velocity Vortex-Type Flow, *J. Heat Transfer*, *79* (1957), 4, pp. 751-758
[4] Ahlborn, B., Gordon, J., The Vortex Tube as a Classical Thermodynamic Refrigeration Cycle, *J. Appl. Phys*, *88* (2000), 6, pp. 645-653
[5] Stephan, K., *et al*., An Investigation of Energy Separation in a Vortex Tube, *Int. J. Heat Mass Transfer*, *26* (1983), 3, pp. 341-348
[6] Kurosaka, M., Acoustic Streaming in Swirling Flows, *J. Fluid Mech*., *124* (1982), 7, pp. 139-172
[7] Aljuwayhel, N. F., Nellis, G. F., Klein, S. A., Parametric and Internal Study of the Vortex Tube Using a CFD Model, *Int. J. Refrig*., *28* (2005), 3, pp. 442-450
[8] Skye, H. M., Nellis, G. F., Klein, S. A., Comparison of CFD Analysis to Empirical Data in a Commercial Vortex Tube, *Int. J. Refrig*., *29* (2006), 1, pp. 71-80
[9] Chang, H. S., Experimental and Numerical Studies in a Vortex Tube, *Journal of Mechanical Science and Technology*, *20* (2006), 3, pp. 418-425
[10] Akhesmeh, S.., Pourmahmoud, N., Sedgi, H., Numerical Study of the Temperature Separation in the Ranque-Hilsch Vortex Tube, *American Journal of Engineering and Applied Sciences*, *1* (2008), 3, pp. 181-187
[11] Eisma-ard, S., Promvonge, P., Numerical Investigations of the Thermal Separation in a Ranque-Hilsch Vortex tube, *Int J Heat Mass Transfer*, *50* (2007), 5-6, pp. 821-832
[12] Kirmaci, V., Optimization of Counter flow Ranque-Hilsch Vortex Tube Performance using Taguchi Method, *International Journal of Refrigeration*, *32* (2009), 7, pp.1487-1494
[13] Hossein, N. A., Shamsoddini, R., Numerical Three-Dimensional Analysis of the Mechanism of Flow and Heat Transfer in a Vortex Tube, *Thermal Science*, *13* (2009), 4, pp. 183-196
[14] Agrawal, A. B., Shrivastava, V., Retrofitting of Vapour Compression Refrigeration Trainer by an Eco-friendly Refrigerant, *Indian J. Sci. Technol*, *3* (2010), 4, pp. 455-458

[15] Jayaraman, B., Senthil Kumar, P., Design Optimisation and Performance Analysis of Orifice Pulse Tube Cryogenic Refrigerators, *Indian J. Sci. Technol*, *3* (2010), 4, pp. 425-436
[16] ***, Vortex Tubes and Spot Cooling Products, Exair Corporation, http://www.exair.com
[17] Gutsol, A. F., The Ranque Effect, *Phys. Uspekhi*, *40* (1997), 6, pp. 639-658
[18] Behera, U., *et al*., CFD Analysis and Experimental Investigations Towards Optimizing the Parameters of Ranque-Hilsch Vortex Tube. *Int. J. Heat Mass Transfer*, *48* (2005), 10, pp. 1961-1973
[19] Fulton, C. D., Ranque's Tube. *J Refrig Eng*, *58* (1950), 5, pp. 473-479
[20] Frohlingsdorf, W., Unger, H., Numerical Investigations of the Compressible Flow and the Energy Separation in the Ranque-Hilsch Vortex Tube, *Int. J. Heat Mass Transfer*, *42* (1999), 3, pp. 415-422

Paper submitted: October 4, 2010
Paper revised: November 23, 2010
Paper accepted: December 24, 2011